On the maximum compactness of neutron stars

Luciano Rezzolla[1,2,3] and Christian Ecker[1]

1 Institut für Theoretische Physik, Goethe Universität, Max-von-Laue-Str. 1,
D-60438 Frankfurt am Main, Germany
2 CERN, Theoretical Physics Department, 1211 Geneva 23, Switzerland
3 School of Mathematics, Trinity College, Dublin, Ireland

Abstract

The stellar compactness, that is, the dimensionless ratio between the mass and radius of a compact star, $\mathcal{C} := M/R$, plays a fundamental role in characterising the gravitational and nuclear-physics aspects of neutron stars. Yet, because the compactness depends sensitively on the unknown equation of state (EOS) of nuclear matter, the simple question: *"how compact can a neutron star be?"* remains unanswered. To address this question, we adopt a statistical approach and consider a large number of parameterised EOSs that satisfy all known constraints from nuclear theory, perturbative Quantum Chromodynamics (QCD), and astrophysical observations. Next, we conjecture that, for any given EOS, the maximum compactness is attained by the star with the maximum mass of the sequence of nonrotating configurations. While we can prove this conjecture for a rather large class of solutions, its general proof is still lacking. However, the evidence from all of the EOSs considered strongly indicates that it is true in general. Exploiting the conjecture, we can concentrate on the compactness of the maximum-mass stars and show that an upper limit appears for the maximum compactness and is given by $\mathcal{C}_{\mathrm{max}} = 1/3$. Importantly, this upper limit is essentially independent of the stellar mass and a direct consequence of perturbative-QCD constraints.

1 Introduction

Neutron stars are prime examples of extremely compact astrophysical objects, where the physical conditions are so extreme that all four fundamental forces of nature play a significant role in determining their structure and dynamics (see, e.g., [1] for a comprehensive collection). When considering neutron stars as static and spherically symmetric solutions of the Einstein equations for a self-gravitating fluid, two quantities are particularly important: the mass M and the radius R. While the masses can be measured to very high precision thanks to accurate radio-pulsar measurements (see, e.g., [2–4]), the radii are known only poorly, mostly because of the complex physics that accompanies their surface emission (see, e.g., [5,6]). The challenges associated with performing a measurement of their size, combined with the enormous theoretical challenges in describing the equation of state (EOS) that regulates their structure and composition, make neutron stars as fascinating as puzzling.

Once an EOS is prescribed, the solution of the Einstein equations for a self-gravitating non-rotating fluid provides an infinite family of equilibrium models characterised by specific values of the mass and radius. A fundamental difference with respect to the equivalent family in Newtonian gravity is that the relativistic (gravitational) mass is upper bounded by a maximum value, M_{TOV} (see, e.g., [7]), where the index "TOV" refers to the Tolman-Oppenheimer-Volkoff equations, whose solution is needed to obtain the equilibria (see, e.g., [8]). Put differently, while equilibrium solutions can be constructed with central energy densities exceeding those corresponding to M_{TOV}, these configurations yield $M < M_{\mathrm{TOV}}$ and are located on the unstable branch of the M-R sequence.

Given the mass and radius of a neutron star, a derived quantity that naturally appears in the properties describing the corresponding spacetime is the compactness defined as

$$\mathcal{C} := \frac{G M}{c^2 R},\qquad(1)$$

where G and c are the gravitational constant and speed of light, respectively. Hereafter, we will adopt geometric units in which $G = 1 = c$, so that the compactness $\mathcal{C} = M/R$ is a dimensionless quantity.

It is well-known in general relativity that the compactness of a static, spherically symmetric, vacuum spacetime is upper bounded by $\mathcal{C} \leq 1/2$, where the equality refers to a black hole described by the Schwarzschild solution. Also well-known in general relativity as the "Buchdahl limit" [9] is that the compactness of a static, spherically symmetric, non-vacuum spacetime is upper bounded by $\mathcal{C} \leq 4/9 =: \mathcal{C}_{\mathrm{Buch}}$ (see also [10] for more general spacetimes). Finally, it is also well-known that when employing microphysical EOSs models to describe the nuclear matter composing neutron stars, the compactness reached are generally smaller than those constrained by the Buchdahl bound, i.e., $\mathcal{C} \sim 0.1 - 0.2$ (see [11] for one of the early studies setting upper limits on the compactness). At the same time, Haensel and Zdunik [12] have argued that the most compact configurations are produced when the low-density part of the EOS is maximally soft, while the high-density is maximally stiff (i.e., with sound speed $c_s = 1$), thus obtaining a maximum compactness of $\mathcal{C} = 0.3543 = 1/2.8294$ [13,14]. This bound is also known as the "causality bound".

The purpose of this work is twofold. First, we propose a conjecture according to which the maximum compactness is achieved by the star with maximum mass, i.e., M_{TOV}. In other words, we conjecture that the star with maximum mass is also the star with the maximum compactness: $\mathcal{C}_{\max} = \mathcal{C}_{\mathrm{TOV}} := M_{\mathrm{TOV}}/R_{\mathrm{TOV}}$. This conjecture can be shown to be mathematically true for some specific non-vacuum spacetimes, for a large class of generic spacetimes, and we provide numerical evidence that it holds for all of the stellar models considered here. Second, we show that when considering EOSs that satisfy constraints derived from nuclear physics and astrophysics, the compactness of *realistic* neutron stars is also upper bounded $\mathcal{C} \leq \mathcal{C}_{\max} < \mathcal{C}_{\mathrm{Buch}}$ and we further determine the value of $\mathcal{C}_{\max}$.

In order to achieve our goals, we will employ a very large set of parameterised EOSs constructed agnostically but such that they satisfy all known constraints derived either from nuclear physics, from perturbative Quantum Chromodynamics (pQCD), gravitational-wave detections, or astrophysical observations of isolated neutron stars. In this way, we show that for all the stellar models in our sample, $\mathcal{C}_{\max} = \mathcal{C}_{\mathrm{TOV}}$ and we provide statistical evidence that $\mathcal{C}_{\max} = 1/3$, in a way that is essentially independent of the stellar mass.

2 Methods

An essential methodological part of our study is represented by the construction of a large set of parameterised EOSs that provide a rich ensemble through which statistical properties and general bounds can be set. The construction of this set of EOSs is made in terms of the parameterisation of the speed of sound and has been presented by [15]. A number of different applications have been made of this ensemble of EOSs [16–19], underlying its validity and versatility.

In practice, our EOSs can be seen as the combination of different parts whose constraints depend on the rest-mass densities considered. More specifically, at the lowest densities, i.e., $n/n_s < 0.5$, – where n and $n_s := 0.16\,\mathrm{fm}^{-3}$ are the baryon number density and the nuclear saturation density, respectively – we use the Baym-Pethick-Sutherland prescription [20] for the crust. In the range $0.5 \leq n/n_s < 1.1$, we randomly sample polytropes to span the range between the softest and stiffest EOSs from [21].[1] At high densities ($n/n_s \approx 40$), corresponding to a baryon chemical potential of $\mu = 2.6\,\mathrm{GeV}$, we impose the pQCD constraint from [24] on the pressure $p(X, \mu)$ of cold quark matter, where the renormalization scale parameter X is sampled uniformly in the range $[1, 4]$.[2] To assess the impact of the pQCD constraint on $\mathcal{C}_{\max}$, we also construct a separate ensemble in which this constraint is not imposed and finding considerable differences (see below). For the intermediate density range ($1.1\,n_s < n \lesssim 40\,n_s$), we follow [26] and model the sound speed as piecewise-linear segments of the chemical potential

$$c_s^2(\mu) = \frac{(\mu_{i+1} - \mu)\,c_{s,i}^2 + (\mu - \mu_i)\,c_{s,i+1}^2}{\mu_{i+1} - \mu_i}\,, \tag{2}$$

where μ_i and $c_{s,i}^2$ are parameters defining the i-th segment in the range $\mu_i \leq \mu \leq \mu_{i+1}$. The number density is then computed as

$$n(\mu) = n_1 \exp\left(\int_{\mu_1}^{\mu} \frac{d\mu'}{\mu' c_s^2(\mu')}\right)\,, \tag{3}$$

---

[1]It is in principle possible to use results from chiral effective field theory to extend to $n/n_s \simeq 2$ the constraints for the low-density part of the EOSs (see, e.g., [22]), albeit with singificantly larger relative errors. Although we find no change in our results when considering the subset of EOSs that are compatible with such constraints [23], we here prefer to employ a more conservative upper limit of $n/n_s = 1.1$ because of the smaller relative errors.

[2]This constraint is by construction compatible with the integral constraint recently proposed by [25].
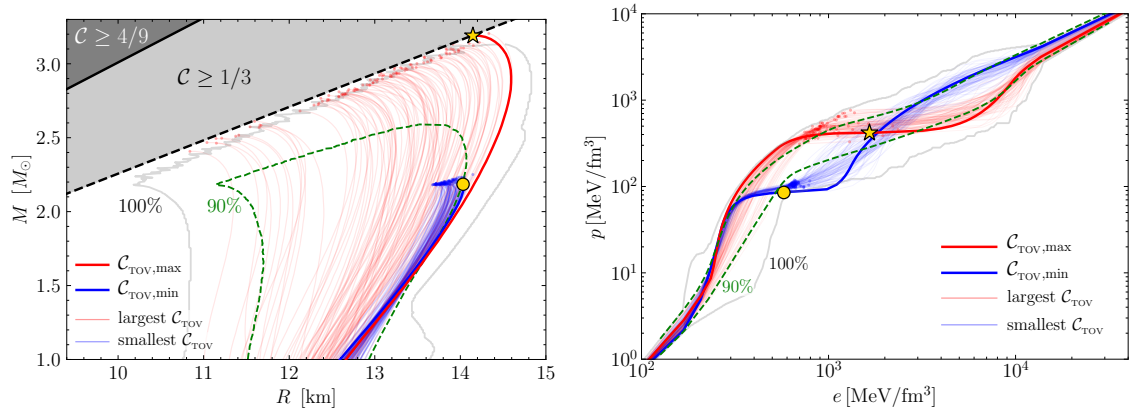
Figure 1: *Left panel:* behaviour in the (M, R) space of the sequences of nonrotating stars with EOSs leading to maximum-mass stars with the largest (smallest) compactness $\mathcal{C}_{\text{TOV,max}}$ ($\mathcal{C}_{\text{TOV,min}}$). Thin red (blue) lines refer to EOSs near the maximum (minimum) compactness, which is instead indicated with a thick red (blue) line. A golden star (circle) marks the position in the (M, R) space of the star with the maximum (minimum) compactness of $\mathcal{C}_{\text{max}} \simeq 0.3329$ ($\mathcal{C}_{\text{min}} \simeq 0.2294$) in the whole ensemble. Also shown with a solid grey (green dashed) line are the contours of the allowed ranges when considering 100% (90%) of the stars in the ensemble. Finally, shown with dark (light) grey shaded areas are the regions where $\mathcal{C} \geq 4/9$ ($\mathcal{C} \geq 1/3$). *Right panel:* the same as on the left but in the (p, e) space.

where $n_1 = 1.1\,n_s$, and $\mu_1 = \mu(n_1)$ is set by the corresponding polytropic EOS. The (isotropic) pressure[3] is obtained via

$$p(\mu) = p_1 + \int_{\mu_1}^{\mu} d\mu'\, n(\mu'), \tag{4}$$

where the integration constant p_1 matches the pressure of the polytrope at $n = n_1$, and we integrate Eq. (4) numerically using seven segments for $c_s^2(\mu)$ (see [15] for a discussion).

Using this framework, we generate approximately 3×10^5 EOSs by randomly sampling the free parameters $\mu_i \in [\mu_1, \mu_{N+1}]$ (where $\mu_{N+1} = 2.6\,\text{GeV}$) and $c_{s,i}^2 \in [0, c_{s,\text{max}}^2]$ with uniformly distributed maximal sound speed $c_{s,\text{max}}^2 \in [0, 1]$ to mitigate the undersampling of low sound-speed values. These EOSs are, by construction, consistent with nuclear theory and pQCD uncertainties, and sufficiently numerous to reach the statistical significance needed for our analysis. Also, while we do not explicitly introduce strong first-order phase transitions for which $c_s^2 = 0$, EOSs closely approximating first-order phase transitions, i.e., with $c_s^2 \sim 0.01 - 0.1$, are naturally present in our ensemble as a result of the uniform sampling in the sound speed. At the same time, when including the extensive coverage of suitably chosen EOSs studied by [29], we find that our results apply unchanged also in the presence of strong first-order phase transitions.

For any EOS in our sample, we can then construct a sequence of nonrotating stellar equilibria by solving the coupled set of TOV equations

$$\frac{dp(r)}{dr} = -\frac{[p(r) + e(r)]\big[\mathcal{C}(r) + 4\pi r^2 p(r)\big]}{r\,[1 - 2\mathcal{C}(r)]} = c_s^2 \frac{de(r)}{dr}, \tag{5}$$

$$m(r) = 4\pi \int_0^r e(r')\, r'^2\, dr', \tag{6}$$

---

[3]We note that we are not considering here anisotropic-pressure contributions as these would very naturally lead to compactnesses that are large and even compatible with those of black holes (see, e.g., [27, 28]).

where $m(r)$ is the gravitational mass within the two-sphere of radius r and $\mathcal{C}(r) := m(r)/r$ with $r \leq R$. The last equality in Eq. (5) employs the definition of the adiabatic sound speed $c_s^2 := (dp/de)_s$. In this way, we are able to construct 2×10^8 nonrotating stellar models in equilibrium, but, of course, not all of these stellar configurations satisfy the present astrophysical constraints. The latter can be expressed in terms of the the mass measurements of J0348+0432 ($M = 2.01 \pm 0.04\,M_\odot$; [30]) and J0740+6620 ($M = 2.08 \pm 0.07\,M_\odot$; [31,32]) and the black-widow binary pulsar PSR J0952-0607 ($M = 2.35 \pm 0.17\,M_\odot$; [33]), which we impose by discarding EOSs yielding a maximum mass $M_{\mathrm{TOV}} < 2.18\,M_\odot$. In addition, we impose the NICER radius constraints from J0740+6620 [34,35] and J0030+0451 [5,6], rejecting EOSs with $R < 10.75\,\mathrm{km}$ at $M = 2.0\,M_\odot$ or $R < 10.8\,\mathrm{km}$ at $M = 1.1\,M_\odot$. Finally, we impose an upper bound on the binary tidal deformability $\tilde{\Lambda}$ as deduced from GW170817 by rejecting all EOSs with $\tilde{\Lambda} > 720$ (low-spin prior; [36]) at a chirp mass $\mathcal{M}_{\mathrm{chirp}} = 1.186\,M_\odot$ for mass ratios $q > 0.73$ (see also [19], where this bound was not imposed in the prior).

We should note that the loss of information following from discarding the uncertainties associated with these measurements is effectively very small, as discussed by [37], who showed that the underlying distributions are almost identical regardless of the choice of constant or variable likelihood, with 90% credible intervals essentially overlapping. Overall, as a result of this additional filtering process, we construct $\approx 1.6 \times 10^7$ stellar models satisfying all the presently known theoretical and astrophysical constraints. These models represent the basis of our statistical analysis.

3 Largest and smallest compactnesses

Using the methodology described above, it is possible to construct probability density functions (PDFs) of the ensemble of stellar models in the relevant space of parameters. The most interesting – and commonly employed – ones are the space of masses and radii, and the space of pressures and energy densities. These PDFs are shown respectively in the left and right panels of Fig. 1. More specifically, for each panel, we show with a solid grey (green dashed) line the contours of the allowed ranges when considering 100% (90%) of the stellar models in the ensemble.

The 100% confidence limits of the distributions in these two spaces have been presented in a number of related works. Here we rather concentrate on those EOSs that lead to the largest and smallest values of the compactness measured for the maximum-mass star, i.e., $\mathcal{C}_{\mathrm{TOV,max}}$ and $\mathcal{C}_{\mathrm{TOV,min}}$, respectively. These are shown with solid thick red and blue lines, while solid thin red and blue lines are used to report the 100 EOSs that have compactnesses close to the largest and smallest ones. Note that each of these lines ends at the maximum-mass star and hence the gold star (circle) marks the position of the stars with the largest (smallest) compactness, while the thin little circles show the corresponding values for the maximum-mass stars that have compactnesses close to the largest/smallest one.

What can be easily appreciated from the left panel of Fig. 1 is that stars with compactnesses near the maximum one actually span very large ranges in radii and masses (thin red lines), with $11\,\mathrm{km} \lesssim R \lesssim 14\,\mathrm{km}$, and $2.3\,M_\odot \lesssim M \lesssim 3.3\,M_\odot$. This behaviour follows from the degeneracy of $\mathcal{C}$. Since the radius of high-mass neutron stars ($M > 2.20\,M_\odot$) can vary significantly, many different mass-radius combinations yield nearly the same compactness. In our analysis, the maximum compactness is attained by all those EOSs whose M–R sequence terminates in the central part of the upper edge of the grey 100% interval shown in the left panel of Fig. 1. By contrast, the spread of the stellar models near the minimum compactnesses (thin blue lines) is very small and the variance in radii is $\lesssim 0.4\,\mathrm{km}$, while that in the mass is $\lesssim 0.1\,M_\odot$. The minimum compactness is clearly determined by the lower mass bound ($M > 2.18\,M_\odot$) imposed

in our analysis, and its value corresponds to the maximum allowed radius at this minimally permitted mass. We also note that if strong first-order phase transition were to be present, then the maximum-mass stars having the smallest-compactness would probably be found at the onset of the phase transition.

To appreciate the origin of the different behaviour for EOSs near $\mathcal{C}_{\text{TOV,max}}$ and $\mathcal{C}_{\text{TOV,min}}$, it is possible to look at the very distinct behaviour of the EOSs associated with stars having maximum/minimum compactnesses. This is shown in the right panel of Fig. 1 using the same convention as in the left panel. Clearly, the maximum-compactness stars (thick and thin red lines) correspond to rather stiff EOSs and the behaviour of the pressure vs energy density essentially borders the 100% confidence contour. Such EOSs typically lead to very massive stars with large-radii and a fraction of them feature structures resembling first-order phase transitions and are responsible for stars being not very massive and with small radii.

On the other hand, the minimum-compactness stars (thick and thin blue lines) correspond to the stiffest EOSs and experience a first-order phase transition (or a rapid cross-over) at comparatively small energy densities. The phase transition leads to an overall softening at large densities and thus to sequences having smaller maximum masses. Naturally, EOSs yielding stars with such large radii but small maximum masses are also characterised by the smallest compactnesses.

Minimally compact stars are clearly realised by EOSs that are stiff at low densities – leading to large neutron star radii – followed by an extended region of low sound speed (i.e., small pressure-vs-energy-density slope), beginning at $e_{\text{PT}} \approx 300 \, \text{MeV/fm}^3$. As indicated by the blue small circles lines, the corresponding maximum central densities of stable neutron stars lie within the flat region around $e_{\text{TOV}} \approx 600 \, \text{MeV/fm}^3$, signalling the termination of their M–R sequence. Conversely, maximally compact EOSs exhibit varying stiffness at lower densities, leading to significant variance in neutron star radii. They feature phase-transition onset densities that are rather large and around $\epsilon_{\text{PT}} \approx 1000 \, \text{MeV/fm}^3$, associated with a phase transition, which typically coincides with e_{TOV}, indicating also in this case that the transition marks the end of their M–R sequence.

4 The most massive is the most compact

Having outlined our methodology, we next advance the conjecture that, once an EOS is fixed, the star with the maximum mass also has the maximum compactness $\mathcal{C}_{\text{max}}$, that is,

$$\mathcal{C}_{\text{max}} = \mathcal{C}_{\text{TOV}} \, . \tag{7}$$

To substantiate this conjecture we use the fact that it is implied by the stronger statement that the compactness is a monotonically growing function of the gravitational mass

$$\frac{d\mathcal{C}(M)}{dM} = \frac{1}{R(M)} \left(1 - \frac{d\ln R}{d\ln M} \right) \geq 0 \, . \tag{8}$$

Although the conjecture (7) appears very natural and almost intuitive, a rigorous analytical proof is lacking, at least to the best of our knowledge. The root of the problem is in assessing whether the term $d\ln R/d\ln M$ on the right-hand side of Eq. (8) is larger or smaller than unity. In turn, this requires the integration of Eq. (6), which would provide a relation $M = M(R)$ (or, equivalently $R = R(M)$) for a generic EOS. Even when making the additional assumption that the energy density is monotonically decreasing with r inside the star, its nonlinear behaviour prevents one from deriving a mathematical proof that $d\ln R/d\ln M < 1$. This difficulty can also be cast in geometric terms: assessing the size of $d\ln R/d\ln M$ amounts to measuring the slope of the growth of the gravitational mass as a function of radius $M = M(R)$ in a (M, R)
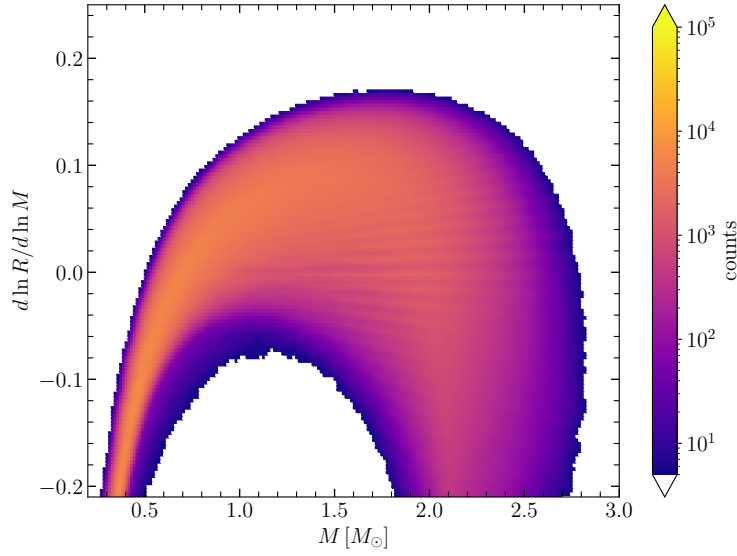
Figure 2: Distribution of the logarithmic derivative $d \ln R / d \ln M$ for all of the stellar models in our ensemble shown as a function of the stellar mass. Since $d \ln R / d \ln M \lesssim 0.18$, for each EOS the most massive star is also the most compact one.

space (see also [38] for a study of the slope in agnostic EOSs). As shown in the left panel of Fig. (1), this slope can vary considerably from EOS to EOS and even change sign when an increase in the mass leads to stellar models with smaller radii.

That said, some progress can be made either considering specific analytic solutions or by restricting the mathematical proof to a general class of possible solutions (see End Matter). We start from the former and consider a star with constant energy density e_c, or "Schwarzschild star". In this case, the mass is simply given by $M = (4\pi/3) e_c R^3$, so that $d \ln R / d \ln M = 1/3$, and thus $d\mathcal{C}/dM = (2/3)R > 0$. The second simple analytic example in support of the conjecture is offered by the Tolman-VII (T-VII) solution [39], that is often invoked as convenient and analytic example of a compact star with properties that are not too far from realistic neutron stars (see, e.g., [40]). We recall that the energy density in a "generalised" T-VII solution is given by [41] $e(r) = e_c(1 - \alpha r^2/R^2)$, where $0 \le \alpha \le 1$ is a constant introduced to modify the "self-boundness" and generalise the original T-VII solution. Clearly $\alpha = 1$ corresponds to the original T-VII solution and $\alpha = 0$ provides the Schwarzschild star.[4] A bit of algebra then shows that the relation between the mass and the radius is given by $M = (4\pi/3)(1 - \alpha/5)e_c R^3$, so that, again, $d \ln R / d \ln M = 1/3$, and thus $d\mathcal{C}/dM = (2/3)R > 0$, independent of the value of α.

Although the generalised T-VII solution offers a very good approximation to a realistic neutron star, it does not exhaust all of the possible behaviours of the energy density $e = e(r)$ and hence of the function $M = M(R)$ for an arbitrary but consistent EOS. As a result, unable to prove the validity of the conjecture (7) in general, we verify it by simply computing the logarithmic slope $d \ln R / d \ln M$ for all of the stellar models constituting our ensemble. This is shown in Fig. 2, which reports with colormap the distribution of the logarithmic derivative $d \ln R / d \ln M$ as a function of the stellar mass. Clearly, since $d \ln R / d \ln M \lesssim 0.18$ across all the relevant range of masses, the function $\mathcal{C}(M)$ is monotonically increasing with mass and the conjecture $\mathcal{C}_{\text{max}} = \mathcal{C}_{\text{TOV}}$ is satisfied by all the stellar models considered here. While this result

---

[4]Note that the energy-density profile of the generalised T-VII solution is not necessarily zero at the stellar surface and, indeed, $e(R) = e_c(1 - \alpha)$, being zero only for $\alpha = 1$, i.e., the original T-VII solution.
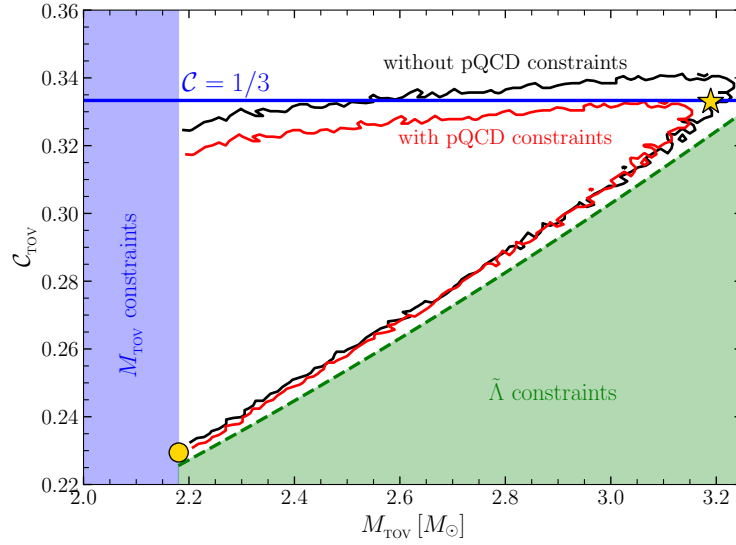
Figure 3: Distribution of the maximum compactness $\mathcal{C}_{\text{TOV}}$ as a function the maximum mass M_{TOV}. Shown as blue- and red-shaded areas are the constraints coming from the maximum mass and the binary tidal deformability, respectively. Also reported with a red dashed line is the analytic fit (9) for the minimum of the maximum-mass compactness $\mathcal{C}_{\text{TOV,min}}$, while the star and circle are the same models as in Fig. 1. The outer bounds without imposing the pQCD constraints is shown with the black solid contour, while the horizontal red solid line marks $\mathcal{C} = 1/3$, highlighting that all stellar models are below this limit when the pQCD constraint is imposed.

does not have the rigour of a mathematical proof, it does provide very strong evidence that, for neutron-star models constructed with EOSs satisfying all known physical and astrophysical constraints, the most massive stars are also the most compact ones.

5 An upper limit on the compactness

Having shown the validity of the conjecture (7) about the maximum compactness, it is now possible to assess whether a global upper limit exists to $\mathcal{C}_{\text{max}}$. To this scope, all is needed is to explore the distribution of the maximum-mass compactness $\mathcal{C}_{\text{TOV}}$ for the ensemble of stellar models built. This is shown in Fig. 3, that reports with a colormap the distribution of the maximum-mass compactness as a function of the maximum mass M_{TOV}.

A rapid inspection of Fig. 3 reveals that the compactness of the maximum-mass stars – and hence the maximum compactness for a given EOS – has a clear upper limit and that this is given by $\mathcal{C}_{\text{max}} \simeq 0.3329 < 1/3$. Importantly, this limit is essentially independent of the stellar mass and hence applies equally to stars with maximum masses ranging from $M_{\text{TOV}} \sim 2.2$ to $M_{\text{TOV}} \sim 3.0 \, M_\odot$. Also important is that this upper limit is essentially determined by the pQCD constraints, which effectively prevent to have stars with very large masses and comparatively small radii. Indeed, stars with $\mathcal{C} > 1/3$ can be found when the pQCD constraint is not imposed and as indicated with the black solid contour in Fig. 3.

Reported instead with a blue-shaded area is the region of the $(\mathcal{C}_{\text{TOV}}, M_{\text{TOV}})$ space that is constrained by the choice of the lower limit for M_{TOV}, so that the blue-shaded area moves to the right for larger values of the assumed minimum value of M_{TOV} (2.18 $M_\odot$ here). Finally, marked with a red-shaded area is the region constrained by the limits deduced on the binary tidal deformability $\tilde{\Lambda}$, which is here set by the GW170817 event. The upper bound of the red-

shaded area, which marks the lower limit in the maximum-mass compactness $\mathcal{C}_{\mathrm{TOV,min}}$. This limit is well-captured by the quadratic relation

$$\mathcal{C}_{\mathrm{TOV,min}} = c_1 + c_2\,\bar{M}_{\mathrm{TOV}} + c_3\,\bar{M}_{\mathrm{TOV}}^2\,, \tag{9}$$

where $\bar{M}_{\mathrm{TOV}} := \bar{M}_{\mathrm{TOV}}/M_{\odot}$, and the fitting coefficients are given by $c_1 = 0.100$, $c_2 = 0.031$, $c_3 = 0.012$. Note that expression (9), which is shown with a thick red dashed line in Fig. 3, improves a similar expression computed by [42] making use of the quasi-universal relation between the maximum-mass of rotating and nonrotating configurations [43]. This lower bound is determined by constraints on tidal deformability and the resulting upper limits on neutron-star radii inferred from GW170817.

Overall, the results presented in Fig. 3 lead to the conclusion that the maximum compactness of neutron-star models satisfying all known physical and astrophysical constraints is given by $\mathcal{C}_{\mathrm{max}} = 1/3$, with the latter value determined by the pQCD constraint.

6 Conclusions

Despite the significant recent progress, the knowledge of the properties of matter in neutron stars still suffers from large uncertainties. As a result, a number of different EOSs have been derived under a variety of assumptions and techniques, and all of these are routinely adopted when modelling the structure and dynamics of neutron stars. Given these difficulties, and at least at zero temperatures, it is possible to approach the problem of the EOS from a purely statistical point of view by generating a large ensemble of physically plausible EOSs constructed so as to satisfy all the known physical constraints. In this way, despite the large uncertainties, a number of robust results can be drawn simply on statistical grounds.

Within this framework, we have considered a very basic and yet unanswered question: *how compact can a neutron star be?* We have addressed this question by populating a very large ensemble of nonrotating stellar models that are constructed making use of EOSs that satisfy all known physics constraints. In addition, the population of stellar models produced from such EOSs is further refined by imposing constraints coming from astronomical observations. However, on the way to address the question above, we have been faced with a related and equally basic question: *given an EOS, which star is the most compact one?* Surprisingly, a simple answer does not exist to the best of our knowledge and thus we conjectured that, given an EOS, the most massive star along the sequence of equilibria is also the most compact or, equivalently, that $\mathcal{C}_{\mathrm{max}} = \mathcal{C}_{\mathrm{TOV}}$. This rather natural conjecture can be proven to be true for some analytic solutions and also for a generic family of stellar models, but remains unproven in general. Luckily, the availability of our large ensemble of stellar models has allowed us to prove, at least numerically, that the conjecture is indeed true across our ensemble. The importance of the conjecture is that it has allowed us to restrict our attention on the compactness of the maximum-mass stars, which represent a much smaller set of stellar models to consider. In this way, we have realised that the maximum compactness for a given EOS has a clear upper limit that is almost independent of the mass considered and given by $\mathcal{C}_{\mathrm{max}} < 1/3$. Because this bound does not appear when the pQCD constraints are not imposed, it represents an intriguing imprint of pQCD at neutron-star densities and of the softening that it induces at the highest densities and pressures [15,44]. In turn, the (unlikely) observation of a neutron star with compactness violating this bound would represent a terrific opportunity to reconsider critically the basic assumptions made in its derivation.

Acknowledgments

It is a pleasure to thank C. Providencia, K. Kokkotas, J. Schaffner-Bielich, and A. Sedrakian for useful discussions. We are also grateful to V. Dexheimer and V. Noronha-Hostler for kindly sharing the set of EOSs published by [29].

Funding information Partial funding comes from the ERC Advanced Grant "JETSET: Launching, propagation and emission of relativistic jets from binary mergers and across mass scales" (Grant No. 884631). CE acknowledges support by the Deutsche Forschungsgemeinschaft (DFG, German Research Foundation) through the CRC-TR 211 "Strong-interaction matter under extreme conditions"– project number 315477589 – TRR 211. LR acknowledges the Walter Greiner Gesellschaft zur Förderung der physikalischen Grundlagenforschung e.V. through the Carl W. Fueck Laureatus Chair.

A A simple but partial proof of the conjecture

In the main text we have discussed how it is hard to prove analytically the validity of the conjecture (7), although we do not exclude that a proof is possible. However, we do provide here the mathematical details that allow to prove the validity of the conjecture (7) for a specific but sufficiently general class of stellar models. In particular, we will consider a broken power law where dM/dR changes sign at a given mass M_* and radius R_*, much like the behaviour shown by most of the EOSs in the left panel of Fig. 1. For convenience, we cast this result in terms of the following theorem.

Theorem. Given a perfect fluid described by a barotropic equation of state, the solutions of the Einstein equations leading to static and spherically symmetric equilibrium configurations with mass M, radius R, and compactness $\mathcal{C} := M/R$, are such that the stellar model with the maximum mass M_{TOV} is also the most compact one when

$$M(R) = \begin{cases} \kappa_1 R^p, & \text{for} \quad M \leq M_*, \\ \kappa_2 R^{-q}, & \text{for} \quad M \geq M_*, \end{cases} \tag{A.1}$$

where κ_1, κ_2, p and q are real and positive constants. Imposing continuity at M_* then constraints $\kappa_2 = \kappa_1 R_*^{p+q}$, where R_* is the radius where $M(R_*) = M_*$.

Proof. We proceed along the same logical route anticipated in the main text, that is, by proving that the compactness is a monotonically growing function such that $\mathcal{C}_{\max} = \mathcal{C}_{\text{TOV}}$. In turn, this implies proving that [see Eq. (8)]

$$\frac{d \ln R}{d \ln M} \leq 1. \tag{A.2}$$

Using the proposed general scaling (A.1), it is the simple to compute that

$$\frac{d \ln R}{d \ln M} = \begin{cases} 1/p, & \text{for} \quad M \leq M_*, \\ -1/q, & \text{for} \quad M \geq M_*, \end{cases} \tag{A.3}$$

so that the condition (A.2) [and hence the conjecture (7)] is satisfied if

$$\begin{cases} p \geq 1, & \text{for} \quad M \leq M_*, \\ q \geq -1, & \text{for} \quad M \geq M_*. \end{cases} \tag{A.4}$$

A few comments are worth making, some of which can be seen as corollaries of the theorem.

- The scaling (A.1) is only a sufficient condition for the validity of the conjecture (7).

- The scaling (A.1) is of class $\mathscr{C}^0$ at R_*, i.e., continuous but with discontinuous derivatives. If useful, additional scaling terms can be introduced to guarantee also continuity of the higher derivatives.

- The generalised T-VII solution represents a special case of the class (A.1) for $M_* \to \infty$ and $p = 3$. Using the condition (A.4), it is simple to deduce that the generalised T-VII solution trivially satisfies the conjecture (7).

- A modification of the T-VII solution has also been proposed in which the behaviour of the energy density is extended by the introduction of a quartic term [45]

$$e(r) = e_c \left(1 - \tilde{\alpha}\, r^2/R^2 - (\tilde{\alpha} - 1) r^4/R^4 \right). \tag{A.5}$$

This solution is also referred to as the "modified" T-VII solution and $\tilde{\alpha} \in [0, 2]$ is a new parameter such that $\tilde{\alpha} = 1$ leads to the generalised T-VII solution and $\tilde{\alpha} = 0$ to the Schwarzschild solution (see [46] for a discussion of the role played by $\tilde{\alpha}$). Although expression (A.5) may appear more complex, it is easy to show that it effectively belongs to the class (A.1) with $M_* \to \infty$ and $p = 3$. Hence, also the modified T-VII solution trivially satisfies the conjecture (7).

- Although the generalised T-VII solution does not have a maximum mass, the Buchdahl limit constraints the central energy density to be

$$e_c < \frac{1}{3\pi R^2 (1 - 3\alpha/5)}, \tag{A.6}$$

so that, even in the absence of a maximum-mass star, it is still true that the most massive star is also the most compact one. The same conclusion is true for the modified T-VII solution, in which case the limit on the central energy density reads

$$e_c < \frac{1}{3\pi R^2 \left[1 - 3\tilde{\alpha}/5 + 3(\tilde{\alpha} - 1)/7 \right]}. \tag{A.7}$$

B More on the largest and smallest compactnesses

In the main text we have discussed some of the properties of the stellar models belonging to the class of EOSs leading the largest and smallest values of the maximum-mass compactnesses, i.e., $\mathcal{C}_{\mathrm{TOV,max}}$ and $\mathcal{C}_{\mathrm{TOV,min}}$. We have also employed Fig. 1 to show the properties of such EOSs in terms of their behaviour in the (M, R) and (p, e) spaces; we here use Fig. 4 to provide some additional information. More specifically, using the same colour and line-style conventions adopted in Fig. 1, the left panel of Fig. 4 reports the behaviour of the square of the sound speed as a function of the energy density, where it is very easy to realise that the EOSs leading to the maximum compactness have a rapid cross-over – as indicated by the sound speed dropping to very small values – only at very large energy densities, thus leading to hybrid stars with a very small quark core. By contrast, the EOSs leading to the minimum compactness have a first-order phase transition already at very low energy densities (in both cases $c_s^2 \to 1/3$ for $n \gg n_s$).

The right panel of Fig. 4 shows instead the functional behaviour of the conformal anomaly $\Delta := 1/3 - p/e$, where p is the pressure, and where $-2/3 \leq \Delta \leq 1/3$ for thermodynamical stability (we recall that $\Delta \to 0$ for $n \gg n_s$). Worth noting in this case is that the conformal anomaly is always positive for EOSs with compactnesses around $\mathcal{C}_{\mathrm{TOV,min}}$, while it becomes negative in large portions of the star for EOSs with compactnesses close to $\mathcal{C}_{\mathrm{TOV,max}}$; this is a behaviour already noted in a number of papers (see, e.g., [17, 47, 48]).
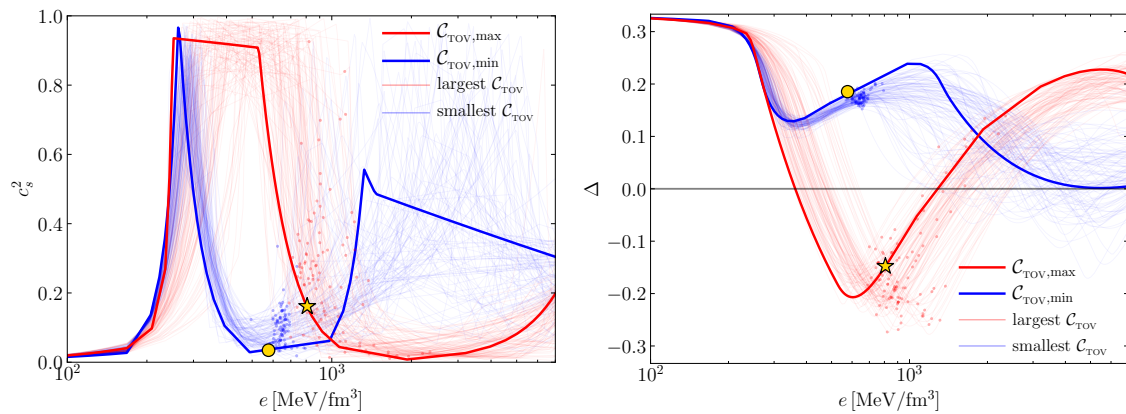
Figure 4: The same as in Fig. 1 but for the behaviour of the sound speed (left panel) and of the conformal anomaly as a function of the energy density (right panel).

References

[1] L. Rezzolla, P. Pizzochero, D. I. Jones, N. Rea and I. Vidaña (eds.), *The physics and astrophysics of neutron stars*, Springer, Cham, Switzerland, ISBN 9783319976150 (2018), doi:10.1007/978-3-319-97616-7.

[2] J. Antoniadis et al., *A massive pulsar in a compact relativistic binary*, Science **340**, 1233232 (2013), doi:10.1126/science.1233232 [preprint doi:10.48550/arXiv.1304.6875].

[3] H. T. Cromartie et al., *Relativistic Shapiro delay measurements of an extremely massive millisecond pulsar*, Nat. Astron. **4**, 72 (2019), doi:10.1038/s41550-019-0880-2 [preprint doi:10.48550/arXiv.1904.06759].

[4] E. Fonseca et al., *Refined mass and geometric measurements of the high-mass PSR J0740+6620*, Astrophys. J. Lett. **915**, L12 (2021), doi:10.3847/2041-8213/ac03b8 [preprint doi:10.48550/arXiv.2104.00880].

[5] T. E. Riley et al., *A NICER view of PSR J0030+0451: Millisecond pulsar parameter estimation*, Astrophys. J. Lett. **887**, L21 (2019), doi:10.3847/2041-8213/ab481c [preprint doi:10.48550/arXiv.1912.05702].

[6] M. C. Miller et al., *PSR J0030+0451 mass and radius from NICER data and implications for the properties of neutron star matter*, Astrophys. J. Lett. **887**, L24 (2019), doi:10.3847/2041-8213/ab50c5 [preprint doi:10.48550/arXiv.1912.05705].

[7] C. W. Misner, K. S. Thorne and J. A. Wheeler, *Gravitation*, W. H. Freeman, San Francisco, USA, ISBN 9780716703440 (1973).

[8] L. Rezzolla and O. Zanotti, *Relativistic hydrodynamics*, Oxford University Press, Oxford, UK, ISBN 9780191746505 (2013), doi:10.1093/acprof:oso/9780198528906.001.0001.

[9] H. A. Buchdahl, *General relativistic fluid spheres*, Phys. Rev. **116**, 1027 (1959), doi:10.1103/PhysRev.116.1027.

[10] N. Dadhich and S. Chakraborty, *Buchdahl compactness limit for a pure Lovelock static fluid star*, Phys. Rev. D **95**, 064059 (2017), doi:10.1103/PhysRevD.95.064059 [preprint doi:10.48550/arXiv.1606.01330].

[11] L. Lindblom, *Limits on the gravitational redshift form neutron stars*, Astrophys. J. **278**, 364 (1984), doi:10.1086/161800.

[12] P. Haensel and J. L. Zdunik, *A submillisecond pulsar and the equation of state of dense matter*, Nature **340**, 617 (1989), doi:10.1038/340617a0.

[13] S. Koranda, N. Stergioulas and J. L. Friedman, *Upper limits set by causality on the rotation and mass of uniformly rotating relativistic stars*, Astrophys. J. **488**, 799 (1997), doi:10.1086/304714 [preprint doi:10.48550/arXiv.astro-ph/9608179].

[14] J. M. Lattimer and M. Prakash, *The equation of state of hot, dense matter and neutron stars*, Phys. Rep. **621**, 127 (2016), doi:10.1016/j.physrep.2015.12.005 [preprint doi:10.48550/arXiv.1512.07820].

[15] S. Altiparmak, C. Ecker and L. Rezzolla, *On the sound speed in neutron stars*, Astrophys. J. Lett. **939**, L34 (2022), doi:10.3847/2041-8213/ac9b2a [preprint doi:10.48550/arXiv.2203.14974].

[16] C. Ecker and L. Rezzolla, *A general, scale-independent description of the sound speed in neutron stars*, Astrophys. J. Lett. **939**, L35 (2022), doi:10.3847/2041-8213/ac8674 [preprint doi:10.48550/arXiv.2207.04417].

[17] C. Ecker and L. Rezzolla, *Impact of large-mass constraints on the properties of neutron stars*, Mon. Not. R. Astron. Soc. **519**, 2615 (2022), doi:10.1093/mnras/stac3755 [preprint doi:10.48550/arXiv.2209.08101].

[18] C. Musolino, C. Ecker and L. Rezzolla, *On the maximum mass and oblateness of rotating neutron stars with generic equations of state*, Astrophys. J. **962**, 61 (2024), doi:10.3847/1538-4357/ad1758 [preprint doi:10.48550/arXiv.2307.03225].

[19] S. J. Magnall, C. Ecker, L. Rezzolla, P. D. Lasky and S. R. Goode, *Physics-informed priors improve gravitational-wave constraints on neutron-star matter*, Astrophys. J. Lett. **988**, L75 (2025), doi:10.3847/2041-8213/adef39 [preprint doi:10.48550/arXiv.2504.21526].

[20] G. Baym, H. A. Bethe and C. J. Pethick, *Neutron star matter*, Nucl. Phys. A **175**, 225 (1971), doi:10.1016/0375-9474(71)90281-8.

[21] K. Hebeler, J. M. Lattimer, C. J. Pethick and A. Schwenk, *Equation of state and neutron star properties constrained by nuclear physics and observation*, Astrophys. J. **773**, 11 (2013), doi:10.1088/0004-637X/773/1/11 [preprint doi:10.48550/arXiv.1303.4662].

[22] C. Drischler, R. J. Furnstahl, J. A. Melendez and D. R. Phillips, *How well do we know the neutron-matter equation of state at the densities inside neutron stars? A Bayesian approach with correlated uncertainties*, Phys. Rev. Lett. **125**, 202702 (2020), doi:10.1103/PhysRevLett.125.202702 [preprint doi:10.48550/arXiv.2004.07232].

[23] H. Koehn et al., *From existing and new nuclear and astrophysical constraints to stringent limits on the equation of state of neutron-rich dense matter*, Phys. Rev. X **15**, 021014 (2025), doi:10.1103/PhysRevX.15.021014 [preprint doi:10.48550/arXiv.2402.04172].

[24] E. S. Fraga, A. Kurkela and A. Vuorinen, *Interacting quark matter equation of state for compact stars*, Astrophys. J. **781**, L25 (2014), doi:10.1088/2041-8205/781/2/L25 [preprint doi:10.48550/arXiv.1311.5154].

[25] O. Komoltsev and A. Kurkela, *How perturbative QCD constrains the equation of state at neutron-star densities*, Phys. Rev. Lett. **128**, 202701 (2022), doi:10.1103/PhysRevLett.128.202701 [preprint doi:10.48550/arXiv.2111.05350].

[26] E. Annala, T. Gorda, A. Kurkela, J. Nättilä and A. Vuorinen, *Evidence for quark-matter cores in massive neutron stars*, Nat. Phys. **16**, 907 (2020), doi:10.1038/s41567-020-0914-9 [preprint doi:10.48550/arXiv.1903.09121].

[27] G. Raposo, P. Pani, M. Bezares, C. Palenzuela and V. Cardoso, *Anisotropic stars as ultracompact objects in general relativity*, Phys. Rev. D **99**, 104072 (2019), doi:10.1103/PhysRevD.99.104072 [preprint doi:10.48550/arXiv.1811.07917].

[28] D. Jampolski and L. Rezzolla, *Nested solutions of gravitational condensate stars*, Class. Quantum Gravity **41**, 065014 (2024), doi:10.1088/1361-6382/ad2317 [preprint doi:10.48550/arXiv.2310.13946].

[29] H. Tan, T. Dore, V. Dexheimer, J. Noronha-Hostler and N. Yunes, *Extreme matter meets extreme gravity: Ultraheavy neutron stars with phase transitions*, Phys. Rev. D **105**, 023018 (2022), doi:10.1103/PhysRevD.105.023018 [preprint doi:10.48550/arXiv.2106.03890].

[30] J. Antoniadis et al., *A massive pulsar in a compact relativistic binary*, Science **340**, 1233232 (2013), doi:10.1126/science.1233232 [preprint doi:10.48550/arXiv.1304.6875].

[31] H. T. Cromartie et al., *Relativistic Shapiro delay measurements of an extremely massive millisecond pulsar*, Nat. Astron. **4**, 72 (2019), doi:10.1038/s41550-019-0880-2 [preprint doi:10.48550/arXiv.1904.06759].

[32] E. Fonseca et al., *Refined mass and geometric measurements of the high-mass PSR J0740+6620*, Astrophys. J. Lett. **915**, L12 (2021), doi:10.3847/2041-8213/ac03b8 [preprint doi:10.48550/arXiv.2104.00880].

[33] R. W. Romani, D. Kandel, A. V. Filippenko, T. G. Brink and W. Zheng, *PSR J0952−0607: The fastest and heaviest known galactic neutron star*, Astrophys. J. Lett. **934**, L17 (2022), doi:10.3847/2041-8213/ac8007 [preprint doi:10.48550/arXiv.2207.05124].

[34] M. C. Miller et al., *The radius of PSR J0740+6620 from NICER and XMM-Newton data*, Astrophys. J. Lett. **918**, L28 (2021), doi:10.3847/2041-8213/ac089b [preprint doi:10.48550/arXiv.2105.06979].

[35] T. E. Riley et al., *A NICER view of the massive pulsar PSR J0740+6620 informed by radio timing and XMM-Newton spectroscopy*, Astrophys. J. Lett. **918**, L27 (2021), doi:10.3847/2041-8213/ac0a81 [preprint doi:10.48550/arXiv.2105.06980].

[36] LIGO scientific collaboration and Virgo collaboration: B. P. Abbott et al., *Properties of the binary neutron star merger GW170817*, Phys. Rev. X **9**, 011001 (2019), doi:10.1103/PhysRevX.9.011001 [preprint doi:10.48550/arXiv.1805.11579].

[37] J.-L. Jiang, C. Ecker and L. Rezzolla, *Bayesian analysis of neutron-star properties with parameterized equations of state: The role of the likelihood functions*, Astrophys. J. **949**, 11 (2023), doi:10.3847/1538-4357/acc4be [preprint doi:10.48550/arXiv.2211.00018].

[38] M. Ferreira and C. Providência, *Constraining neutron star matter from the slope of the mass-radius curves*, Phys. Rev. D **110**, 063018 (2024), doi:10.1103/PhysRevD.110.063018 [preprint doi:10.48550/arXiv.2406.12582].

[39] R. C. Tolman, *Static solutions of Einstein's field equations for spheres of fluid*, Phys. Rev. **55**, 364 (1939), doi:10.1103/PhysRev.55.364.

[40] J. M. Lattimer and M. Prakash, *Neutron star structure and the equation of state*, Astrophys. J. **550**, 426 (2001), doi:10.1086/319702 [preprint doi:10.48550/arXiv.astro-ph/0002232].

[41] A. M. Raghoonundun and D. W. Hobill, *Possible physical realizations of the Tolman VII solution*, Phys. Rev. D **92**, 124005 (2015), doi:10.1103/PhysRevD.92.124005 [preprint doi:10.48550/arXiv.1506.05813].

[42] E. R. Most, L. R. Weih and L. Rezzolla, *The heavier the better: How to constrain mass ratios and spins of high-mass neutron star mergers*, Mon. Not. R. Astron. Soc.: Lett. **496**, L16 (2020), doi:10.1093/mnrasl/slaa079 [preprint doi:10.48550/arXiv.2003.10391].

[43] C. Breu and L. Rezzolla, *Maximum mass, moment of inertia and compactness of relativistic stars*, Mon. Not. R. Astron. Soc. **459**, 646 (2016), doi:10.1093/mnras/stw575 [preprint doi:10.48550/arXiv.1601.06083].

[44] T. Gorda, O. Komoltsev and A. Kurkela, *Ab-initio QCD calculations impact the inference of the neutron-star-matter equation of state*, Astrophys. J. **950**, 107 (2023), doi:10.3847/1538-4357/acce3a [preprint doi:10.48550/arXiv.2204.11877].

[45] N. Jiang and K. Yagi, *Improved analytic modeling of neutron star interiors*, Phys. Rev. D **99**, 124029 (2019), doi:10.1103/PhysRevD.99.124029 [preprint doi:10.48550/arXiv.1904.05954].

[46] C. Posada, J. Hladík and Z. Stuchlík, *Dynamical stability of the modified Tolman VII solution*, Phys. Rev. D **103**, 104067 (2021), doi:10.1103/PhysRevD.103.104067 [preprint doi:10.48550/arXiv.2103.12867].

[47] Y. Fujimoto, K. Fukushima, L. D. McLerran and M. Praszałowicz, *Trace anomaly as signature of conformality in neutron stars*, Phys. Rev. Lett. **129**, 252702 (2022), doi:10.1103/PhysRevLett.129.252702 [preprint doi:10.48550/arXiv.2207.06753].

[48] M. Marczenko, L. McLerran, K. Redlich and C. Sasaki, *Reaching percolation and conformal limits in neutron stars*, Phys. Rev. C **107**, 025802 (2023), doi:10.1103/PhysRevC.107.025802 [preprint doi:10.48550/arXiv.2207.13059].